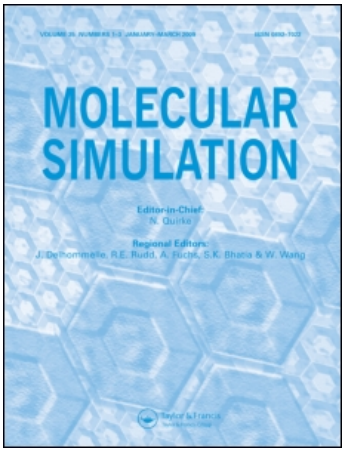

Molecular Simulation
Publication details, including instructions for authors and subscription information:
http://www.informaworld.com/smpp/title~content=t713644482

Lattice Anomaly of MgB (*h*-BN) and Related Compounds under Various Compression Conditions

Kazuaki Kobayashi[a]; Masao Arai[a]
[a] Computational Materials Science Center, National Institute for Materials Science, Ibaraki, Japan

To cite this Article Kobayashi, Kazuaki and Arai, Masao(2004) 'Lattice Anomaly of MgB (*h*-BN) and Related Compounds under Various Compression Conditions', Molecular Simulation, 30: 13, 981 — 986
To link to this Article: DOI: 10.1080/08927020410001709343
URL: http://dx.doi.org/10.1080/08927020410001709343

Molecular Simulation, Vol. 30 (13–15), 15 November–30 December 2004, pp. 981–986

Lattice Anomaly of MgB (*h*-BN) and Related Compounds under Various Compression Conditions

KAZUAKI KOBAYASHI* and MASAO ARAI

Computational Materials Science Center, National Institute for Materials Science, 1-1 Namiki, Tsukuba, Ibaraki 305-0044, Japan

(Received January 2004; In final form March 2004)

We study hexagonal materials of MgB (*h*-BN) and related compounds under various compression conditions. We found the anomalous behavior of lattice constants *a* (*b*) for MgB (*h*-BN) and HBC. Lattice constants *a* of MgB (*h*-BN) and HBC contract under *c*-axis compression. This means that the Poisson ratio is negative. The lattice contraction of *a*-axis is 0.0017 nm for MgB (*h*-BN) when $P_z = 50$ GPa, 0.0002 nm for HBC when $P_z = 20$ GPa. The contraction of HBC is quite small.

Keywords: First-principles; Anisotropic compression; Lattice anomaly; Negative Poisson ratio; Electronic structure

INTRODUCTION

A great deal of effort has been made on high-pressure physics. What seems to be lacking, however, is an approach of anisotropic compression at sufficiently low temperatures. It is impossible to realize that the shock compression experiment is performed at very low temperature although it can apply to samples of materials under anisotropic compression. It is also very difficult to prepare samples as a large single crystal which is adequate to apply under anisotropic compression. In the past, theoretical approaches using the first-principle calculations under anisotropic compression have not often been attempted because of the lack of corresponding high-pressure experiments at sufficiently low temperatures. It is expected that they may predict novel physical properties and behavior of materials under anisotropic compression. We believe that theoretically investigating the electronic and lattice properties of materials under various compression conditions is very important.

Recently, we found the lattice anomalies of LiBC and HBC under anisotropic compression [1–3]. Lattice constant *c* of LiBC and HBC contract under *a*, *b*-axis compression (P_{xy}) although lattice constant *c* generally expands under *a*, *b*-axis compression. This contraction of lattice constant *c* shows a kind of negative Poisson ratio. A mechanism of this anomaly is partially clarified in the previous studies [1–4].

In this study, the electronic and lattice properties of MgB (hexagonal-BN type crystal structure: *h*-BN as $P6_3/mmc$) and related compounds under various compression conditions are calculated using the first-principles molecular dynamics (FPMD) method. MgB (*h*-BN) is a hypothetical compound and has been obtained in the previous study [5]. We have found the lattice anomaly of MgB (*h*-BN) under anisotropic compression [6]. A feature of the lattice anomaly for MgB (*h*-BN) is different from those of the previous results for HBC and LiBC. Lattice constant *a* (*b*) of MgB (*h*-BN) contracts under uniaxial *c*-axis compression (P_z). From the crystal symmetry, lattice of *a* (*a*-axis) is equal to that of *b* (*b*-axis). This contraction of lattice constant *a* shows the negative Poisson ration. As for HBC, we obtain the anomalous behavior of lattice constant *a* under *c*-axis compression, but the value of contraction is quite small. In addition, some hexagonal materials were investigated to search the lattice anomaly under various compression conditions [1–7]. There are no anomalies with the exception of LiBC, HBC and MgB (*h*-BN).

In this study, we try to clarify the origin of the anomaly for MgB (*h*-BN). It is impossible to describe the origin from the same aspect with LiBC [2] and HBC [3] cases. It is likely that the anomaly of lattice

*Corresponding author. E-mail: kobayashi.kazuaki@nims.go.jp

ISSN 0892-7022 print/ISSN 1029-0435 online © 2004 Taylor & Francis Ltd
DOI: 10.1080/08927020410001709343

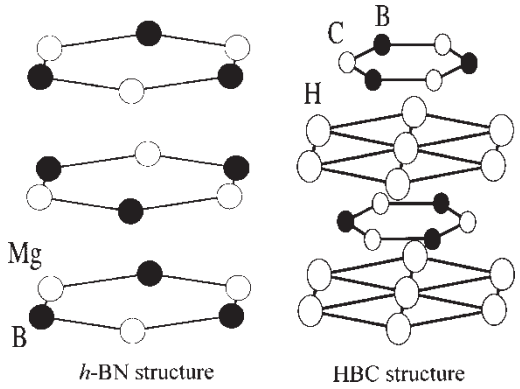

FIGURE 1 Crystal structures of MgB (*h*-BN) and HBC.

constant *a* has relation with the change in the electronic band structure of MgB (*h*-BN) under *c* axis compression.

The outline of this paper is as follows: in the second section Calculation methods are described. Results and discussion are presented in the third section, and Summary is given in the fourth section.

CALCULATIONAL METHODS

The present calculation is based on the local density approximation (LDA) in density functional theory [8,9] with some interpolation formula [10–13] for the exchange-correlation. The optimized pseudopotentials (H, Mg, B and C) by Troullier and Martins (TM) [14,15] are used. Nonlocal parts of the pseudopotentials are transformed to the Kleinman–Bylander separable forms [16] without ghost bands. A partial core correction (PCC) [17] is considered for the Mg pseudopotential. The number of sampling *k*-points is 259 for MgB (*h*-BN) and 95 for HBC in the irreducible Brillouin zone (BZ). The wave function is expanded in plane waves, and the energy cutoff is 81 Ry with the maximum number of plane waves being about 5500 for MgB (*h*-BN). The number of atoms in a unit cell is 4 for MgB (*h*-BN) and 6 for HBC. The crystal structures of MgB (*h*-BN) and HBC are shown in Fig. 1.

The optimization of the electronic and ionic degrees of freedom is performed by a modified version of the FPMD method originally proposed by Car and Parrinello [18]. The optimization of the electronic structure is carried out by using a modified steepest descent type of algorithm as proposed by Williams and Soler [19] in this version. Although the structural optimization is performed using Hellmann–Feynman forces for all atoms in the unit cell, all atoms do not displace due to the imposed crystal symmetry. We treat the hydrostatic, uniaxial (*c*-axis) and bi-axial (*a*, *b*-axis) compression conditions. Stresses acting on the unit cell surfaces are calculated using the formula given in Ref. [20]. The stresses and the lattice parameters (lattice constant and c/a ratio) are tuned by using them. Our criterion for optimizing the unit cell surfaces is that the maximum pressure acting on each unit cell surface should be less than 0.03 GPa, which corresponds to an alteration of less than 0.001 a.u.

TABLE I "○" indicates that lattice constant *c* (*a*) contracts under *a*, *b* (*c*)-axis compression. " × " indicates no lattice anomalies. "*AA*" indicates primitive "*A*-*A*" stacking. "I", "M" and "S" indicate "Insulator", "Metal" and "Semimetal", respectively. "Δ" indicates tentative.

	Pressure				*Pressure*		
LiBC	$P = 0$ GPa	–	I	$LiB_2(AlB_2)$	$P = 0$ GPa	–	M
LiBC	$p_{xy} = 5$ GPa	Small	I	$LiB_2(AlB_2)$	$p_{xy} = 50$ GPa	×	M
LiBC	$p_{xy} = 50$ GPa	○	I	$LiC_2(AlB_2)$	$P = 0$ GPa	–	M
LiBC	$P_{xy} = 100$ GPa	○	I	$Lic_2(AlB_2)$	$p_{xy} = 50$ GPa	×	M
LiBC	$p_{xy} = 200$ GPa	○	I	$MgC_2(AlB_2)$	$P = 0$ GPa	–	M
LiBC	$p_{xy} = 500$ GPa	○	S	$MgC_2(AlB_2)$	$p_{xy} = 50$ GPa	×	M
LiBC	$p_{xy} = 1$ TPa	Δ	M	ZnO(Wurtzite)	$P = 0$ GPa	–	I
LiBC	$p_{xy} = 1.5$ TPa	×	M	ZnO(Wurtzite)	$p_{xy} = 50$ GPa	×	M
LiBC(*AA*)	$P = 0$ GPa	–	S	NaCl(WC)	$P = 0$ GPa	–	I
LiBC(*AA*)	$p_{xy} = 50$ GPa	○	S	NaCl(WC)	$p_{xy} = 50$ GPa	×	I
MgBC	$P = 0$ GPa	–	M	Cd(hcp)	$P = 0$ GPa	–	M
MgBC	$p_{xy} = 20$ GPa	×	M	Cd(hcp)	$p_{xy} = 50$ GPa	×	M
MgBC	$p_{xy} = 50$ GPa	×	M	*h*-BN	$P = 0$ GPa	–	I
NaBC	$P = 0$ GPa	–	I	*h*-BN	$p_{xy} = 50$ GPa	×	I
NaBC	$p_{xy} = 20$ GPa	×	M	Graphite	$P = 0$ GPa	–	S
NaBC	$p_{xy} = 50$ GPa	×	M	Graphite	$p_{xy} = 50$ GPa	Δ	S
$CuScO_2$	$P = 0$ GPa	–		$NaCoO_2$	$P = 0$ GPa	–	
$CuScO_2$	$p_{xy} = 50$ GPa	×		$NaCoO_2$	$p_{xy} = 50$ GPa	×	
Li_3N	$P = 0$ GPa	–	I	Os(hcp)	$p_{xy} = 0$ GPa	–	M
Li_3N	$p_{xy} = 50$ GPa	×	I	Os(hcp)	$p_{xy} = 50$ GPa	×	M
MgB (*h*-BN)	$P = 0$ GPa	–	M	HBC	$p_{xy} = 0$ GPa	–	M
MgB (*h*-BN)	$p_z = 50$ GPa	○	M	HBC	$p_{xy} = 50$ GPa	○	M
MgB (*h*-BN)	$p_z = 500$ GPa	○	M	HBC	$p_{xy} = 100$ GPa	○	M
MgB (*h*-BN)	$p_z = 1$ TPa	×	M	HBC	$p_{xy} = 200$ GPa	×	M
MgB (*h*-BN)	$p_{xy} = 50$ GPa	×	M	HBC	$p_z = 20$ GPa	Δ	M
				HBC	$p_z = 50$ GPa	×	M

TABLE II Optimized lattice constants [nm], the c/a ratios of MgB (*h*-BN) HBC [3] and LiBC[1, 2]. "PBE" indicates the generalized gradient approximation (GGA-PBE) [13].

	Gpa	*c*	*a*	*c/a*
MgB (*h*-BN)	$P = 0$ GPa	0.4564	0.4099	1.11
MgB (*h*-BN)	$p = 50$ GPa	0.4074	0.3530	1.15
MgB (*h*-BN)	$p_{xy} = 50$ GPa	0.4655	0.3479	1.34
MgB (*h*-BN)	$p_z = 50$ GPa	0.4010	0.4082	0.98
MgB (*h*-BN)	$p_z = 100$ GPa	0.3746	0.4048	0.93
MgB (*h*-BN)	$p_z = 200$ GPa	0.3425	0.3988	0.86
MgB (*h*-BN)	$p_z = 500$ GPa	0.2840	0.3929	0.72
MgB (*h*-BN)	$p_z = 1$ TPa	0.2217	0.3963	0.56
HBC	$P = 0$ GPa	0.5796	0.2694	2.15
HBC(PBE)	$P = 0$ GPa	0.5837	0.2672	2.18
HBC	$p = 50$ GPa	0.4968	0.2589	1.92
HBC	$p_{xy} = 50$ GPa	0.5759	0.2573	2.24
HBC	$p_z = 20$ GPa	0.5367	0.2692	1.99
HBC	$p_z = 50$ GPa	0.4865	0.2700	1.80
LiBC	$P = 0$ GPa	0.6950	0.2735	2.54
LiBC	$p = 50$ GPa	0.5870	0.2617	2.24
LiBC	$p_{xy} = 50$ GPa	0.6936	0.2590	2.68
LiBC	$p_z = 50$ GPa	0.5636	0.2761	2.04
LiBC	(Exp [21])	0.7058	0.2752	2.56

in the optimization of the lattice constant. The number of *k*-points is fixed during the cell optimization.

All systems maintain the crystal symmetry under compression. Therefore, lattice dynamics and structural phase transition in a process of the FPMD are not considered in this study. The purpose of our FPMD is to obtain the final stable structure under external compression.

RESULTS AND DISCUSSION

Our present and previous [1–7] results to search lattice anomalies under various compression conditions are tabulated in Table I. Calculated hexagonal materials with the exception of LiBC, HBC and MgB (*h*-BN) do not show the lattice anomalies under all compression conditions (hydrostatic, *a*, *b*-axis and *c*-axis). Lattice constant *c* of graphite contracts when $P_{xy} = 50$ GPa. However, this result should be considered as tentative since the Van der Waals interaction between inter-layers are problematic for the DFT-LDA calculation.

The lattice properties of MgB (*h*-BN), HBC and LiBC are tabulated in Table II. They include previous results [2,3] for comparison with present data. The lattice constants *a* (*b*) of MgB (*h*-BN) contract when $P_z = 50-600$ GPa and HBC when $P_z = 20$ GPa. They expand when $P_z = 700$ GPa for MgB (*h*-BN) and $P_z = 50$ GPa for HBC, respectively. Lattice constant *c* when $P_z = 1$ TPa shrinks to about half of that when $P = 0$ GPa. There are no anomalies for MgB (*h*-BN) under hydrostatic, *a*, *b*-axis compressions. As for MgB (*h*-BN), the values of the lattice parameters converge sufficiently at 259 *k*-points when $P_z = 200$ GPa, at which the deviation of the lattice constant between the results at 259 and 370 *k*-points is less than about 0.001 Å.

Two electronic band structures of MgB (*h*-BN) are shown in Fig. 2(a) and (b). Figure 2(a) is when $P_z = 50$ GPa. For comparison, Fig. 2(b) shows the energy bands with lattice constant *a* chosen at the value when $P = 0$ GPa while *c* is fixed at the value when $P_z = 50$ GPa. There is no difference between two electronic band structures since the contraction is quite small (0.0017 nm).

The electronic band structures of MgB (*h*-BN) when $P = 0, 50$ GPa, $P_{xy} = 50$ GPa and $P_z = 100, 500$ GPa and 1 TPa are shown in Fig. 3. They are metallic under all calculated compression conditions in this study. The bandwidths increase as the pressure increases in all cases. They broadly resemble each other although dispersions of individual bands near the Fermi level differ

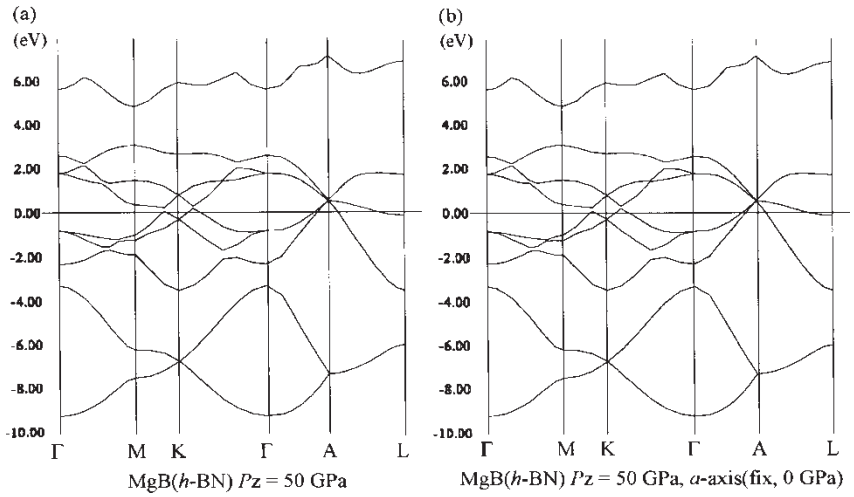

FIGURE 2 Electronic band structures of MgB (*h*-BN) when $P_z = 50$ GPa and lattice constant *a* is chosen at the value when $P = 0$ GPa while *c* is fixed at the value $P_z = 50$ GPa. The Fermi level is indicated by the horizontal line.

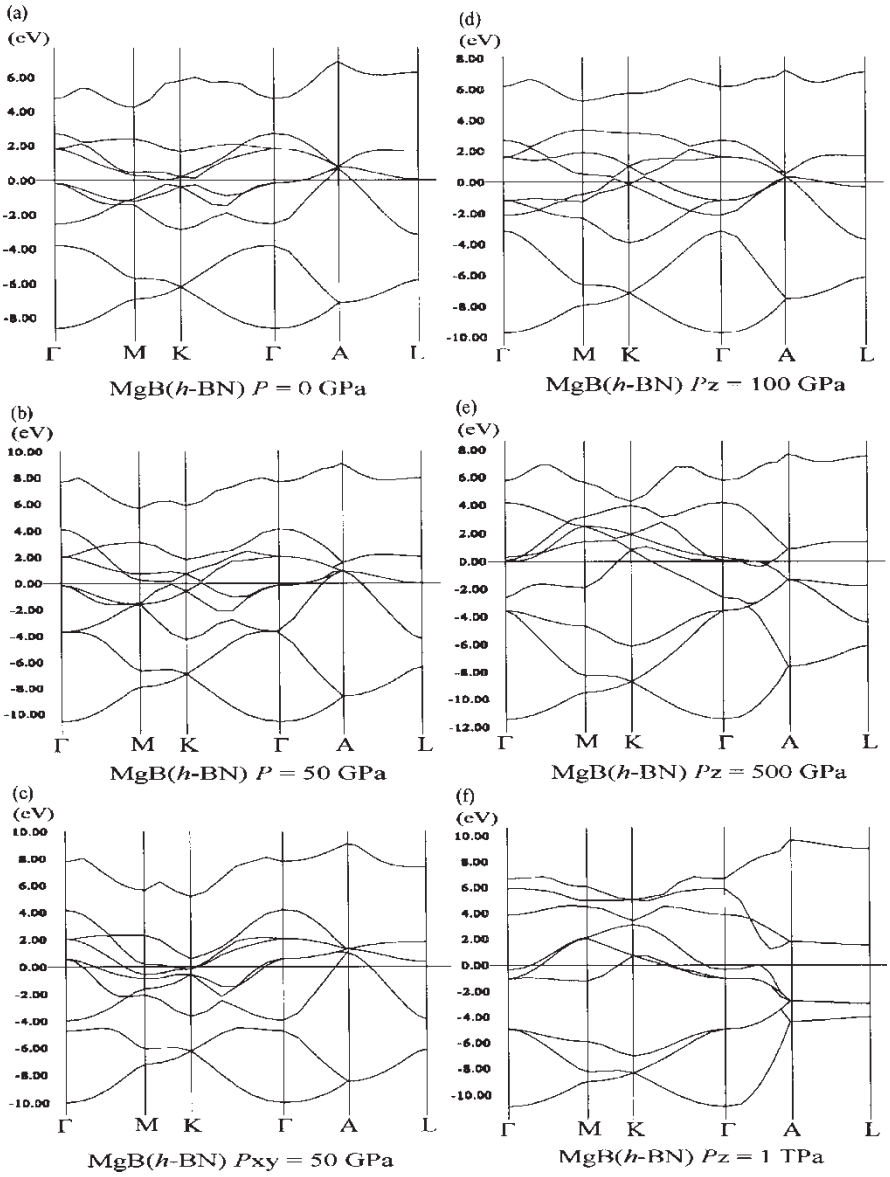

FIGURE 3 Energy band structures of MgB (*h*-BN) when $P = 0, 50$ GPa, $P_{xy} = 50$ GPa and $P_z = 100, 500$ GPa and 1 TPa. The Fermi level is indicated by the horizontal line.

between them as shown in Fig. 3(a)–(d). The change in the electronic band structures near the Fermi level is remarkable when $P_z \geq 300$ GPa. From the electronic band structures when $P_z = 500$ GPa and 1 TPa as shown in Fig. 3(e) and (f), they are quite different from other band structures as shown in Fig. 3(a)–(d).

In previous work [6], we have already considered the origin of this anomalous contraction. However, the reason why lattice constant *a* contracts under *c*-axis compression was not clearly determined. From the crystal structure of MgB (*h*-BN) as shown in Fig. 1, there is no electrostatic inter-layer coupling. We have noticed the change in the electronic band structures under *c*-axis compression. Thus, we have suggested that the contraction of lattice constant *a* (*b*) under *c*-axis compression may have some relation to the change in the electronic band structures [6].

The electronic bands at the *A*-point near the Fermi level are almost invariant when $P = 0, 50$ GPa, $P_{xy} = 50$ GPa and $P_z = 100$ GPa as shown in Fig. 3(a)–(d), respectively. In contrast, the electronic bands around *K*-point near the Fermi level change larger by the compression than those at the *A*-point, with the exception of Fig. 3(e) and (f). The lowest unoccupied band at the *L*-point when $P = 0$ GPa shifts slightly to a lower energy when $P_z = 50$ and 100 GPa and becomes the occupied band under *c*-axis compression as shown in Fig. 3(a) and (d), which may then induce a structural phase transformation. Furthermore, they may have relation to the *a*, *b*-axis contraction under *c*-axis compression. As we have mentioned in the "Calculational methods" section,

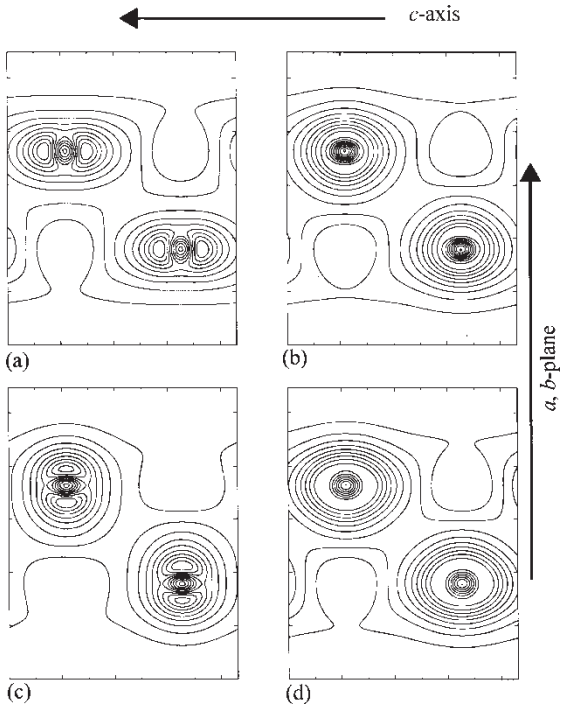

FIGURE 4 Side views of the charge densities for 3rd (a), 4th (b) and 5th (c) bands from the bottom of bands and total charge density (d) when $P = 0$ GPa in a cross section.

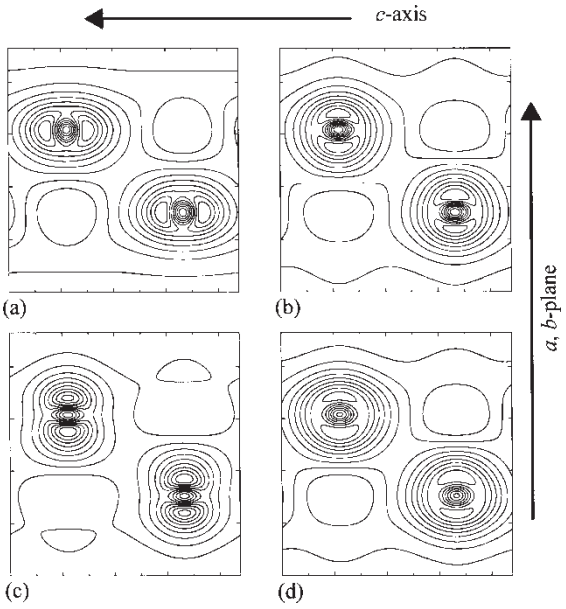

FIGURE 5 Side views of the charge densities for 3rd (a), 4th (b) and 5th (c) bands from the bottom of bands and total charge density (d) when $P_{xy} = 50$ GPa in a cross section.

the structural phase transformation induced by compression is not taken into account in this study.

Two electronic bands cross the Fermi level at the Γ-*A* line when $P = 0$ GPa as shown in Fig. 3(a). They have relation to the Mg—B bonding on the intra-layer. These bands shift to lower energy under *c*-axis compression as shown in Fig. 2(a) and 3(d). Its occupation increases as a result of shifting the lower energy, so that the bond of Mg and B in the intra-layer is strengthened by increasing bonding electrons. In the previous study [6], we have mentioned that it may be the driving force of the *a*, *b*-axis contraction.

We calculate the charge densities of MgB (*h*-BN) when $P = 0$ GPa, $P_{xy} = 50$ GPa and $P_z = 50$ GPa in order to clarify the driving force of the anomalous lattice contraction of *a* (*b*)-axis as show in Fig. 4, 5 and 6. These figures are side views of the charge densities in the cross section of the Mg—B bond. Although we can see the charge densities of boron, those of magnesium are not clear in all cases. The charge densities for the electronic bands, which cross the Fermi level at the Γ-*A* line when $P = 0$ GPa, 3rd, 4th and 5th bands from the bottom of bands are shown in Fig. 4(a), (b) and (c), respectively. The charge densities corresponding to the same bands when $P_{xy} = 50$ GPa and $P_z = 50$ GPa are shown in Fig. 5(a)–(c) and Fig. 6(a)–(c), respectively. The total charge densities are also shown in Figs. 4(d), 5 (d) and 6 (d), respectively.

When $P = 0$ GPa, the bonding charge is not evident in the total charge density as shown in Fig. 4(d). We can see the bonding charge along the *c*-axis when $P_z = 50$ GPa, in which the electron density is redistributed from that when $P = 0$ GPa in the total charge density as shown in Fig. 6(d). This bonding charge induced by *c*-axis compression does not enhance the interaction of the Mg—B bond in the intra-layer.

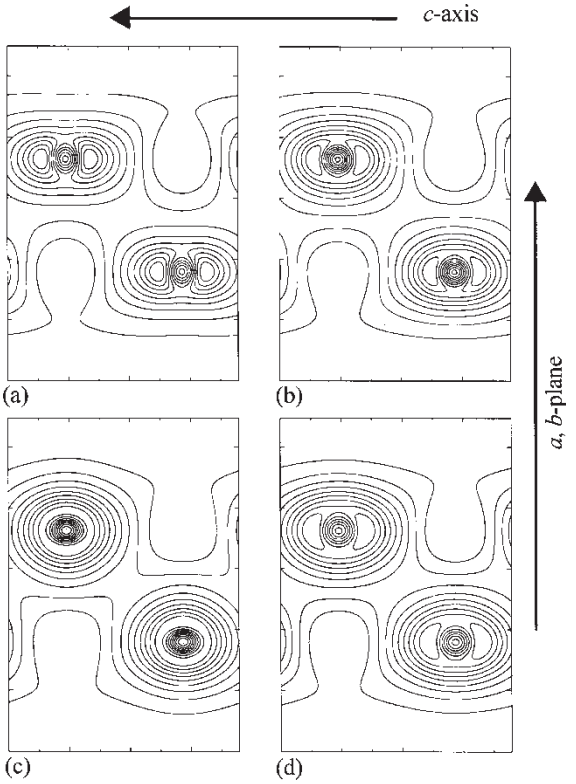

FIGURE 6 Side views of the charge densities for 3rd (a), 4th (b) and 5th (c) bands from the bottom of bands and total charge density (d) when $P_z = 50$ GPa in a cross section.

Furthermore, it seems to enhance the inter-layer coupling. The bonding charges of the intra-layer are not evident in the charge densities of 3rd, 4th and 5th bands as shown in Fig. 6(a)–(c). On the other hand, there are bonding charges along the Mg—B bond of the intra-layer in the 4th, 5th and total charge densities when $P_{xy} = 50$ GPa as shown in Fig. 5(b)–(d). We cannot determine the driving force of the lattice contraction of *a* under *c*-axis compression from the analysis of the charge densities.

SUMMARY

We have calculated MgB (*h*-BN) and related compounds under various compression conditions using FPMD. We found that lattice constants *a* (*b*) of MgB (*h*-BN) and HBC contract under *c*-axis compression These contractions show the negative Poisson ratio. It should be noted that this lattice anomaly does not involve the internal lattice distortion and displacements of atoms in the unit cell. It is confirmed that lattice constant *a* of MgB (*h*-BN) contracts until $P_z = 600$ GPa. It expands from $P_z = 700$ GPa. In contrast, the lattice constant *a* of HBC contracts when $P_z = 20$ GPa and it expands when $P_z = 50$ GPa. The contraction of HBC is very small with 0.0002 nm when $P_z = 20$ GPa. The values of the contraction for MgB (*h*-BN) are 0.0017 nm when $P_z = 50$ GPa, 0.017 nm when $P_z = 500$ GPa. It is necessary to pay attention to the accuracy of lattice parameters depending the number of *k*-points in the order of 0.0001 nm [22]. The number of *k*-points of HBC is 95, which is less than that of MgB (*h*-BN) with 259 *k*-points. That said, the anomaly of HBC may disappear in more detailed calculations.

The contraction of *a* (*b*)-axis in this study is different from the previous results of HBC and LiBC [1–3]. Therefore, the mechanism of the contraction is also different and cannot describe the same way of HBC and LiBC under biaxial (*a*, *b*-axis) compression. From the geometry of MgB (*h*-BN) crystal structure, it is impossible to describe the contraction of lattice constant *a* due to the inter-layer electrostatic interaction and the size of the cation atom [2–4]. The origin of the lattice anomaly of MgB (*h*-BN) under *c*-axis compression has relation to the change in the occupation of bands induced by uniaxial compression. The lattice contraction of *a*-axis under *c*-axis compression is attributed to the increasing of the bonding electrons with increasing the occupation of the band at the Γ-*A* line near the Fermi level.

It is quite difficult to realize the anisotropic compression experimentally at sufficiently low temperatures. There is no way to confirm experimentally this phenomena at present. Actually, it is impossible to compress anisotropically materials keeping the crystal symmetry as pressure is 1 TPa. An effect of core states under such high-pressure conditions is not considered in this study due to the constraint of the pseudopotentials. Furthermore, the FPMD calculations in this study do not take the structural transformation into account in the process of them. More detailed investigation is necessary for HBC under *c*-axis compression. We believe that the theoretical study of anisotropic compression will be more important in the near future.

Acknowledgements

The numerical calculations were performed at NIMS (Namiki, AlphaServer GS140[HP]).

References

[1] Kobayashi, K. and Arai, M. (2003) "LiBC and related compounds under high-pressure", *Physica C* **201**, 388–389.
[2] Kobayashi, K. and Arai, M. (2003) "Lattice anomaly of LiBC and related compounds under anisotropic compression", *J. Phys. Soc. Jpn.* **72**, 217.
[3] Kobayashi, K., Arai, M. and Sasaki, T. (2004) "Lattice Anomalies of *M*BC (*M* = H, Li, Na) Under Anisotropic Compression", in *Proceedings (Trans. MRS-J) of IUMRS-ICAM2003*, submitted.
[4] Arai, M., Kobayashi, K. and Sasaki, T., unpublished.
[5] Kobayashi, K., Arai, M. and Yamamoto, K. (2003) "Electronic and lattice properties of MgB_2 and related phases under various compression conditions", *J. Phys. Soc. Jpn.* **72**, 2886.
[6] Kobayashi, K. and Arai, M. (2004) "Lattice anomaly of MgB (*h*-BN) under anisotropic compression", *Materials Transactions* **45**, in press.
[7] Kobayashi, K. and Arai, M. (2003) "Theoretical search for lattice anamolies of hexagonal materials under anisotropic compression", *in Proceedings of ISAM2003*
[8] Hohenberg, P. and Kohn, W. (1964) "Inhomogeneous electron gas", *Phys. Rev.* **136**, B864.
[9] Kohn, W. and Sham, L.J. (1965) "Self-consistent equations including exchange and correlation effects", *Phys. Rev.* **140**, A1133.
[10] Wigner, E. (1934) "On the interaction of electrons in metals", *Phys. Rev.* **46**, 1002.
[11] Perdew, J. and Zunger, A. (1981) "Self-interaction correction to density-functional approximations for many-electron systems", *Phys. Rev. B* **23**, 5048.
[12] Barth, U.von and Hedin, L. (1972) "A local exchange-correlation potential for the spin polarized case", *J. Phys. C* **5**, 1629.
[13] Perdew, J.P., Burke, K. and Ernzerhof, M. (1906) "Generalized gradient approximation made simple", *Phys. Rev. Lett.* **77**, 3865.
[14] Troullier, N. and Martins, J.L. (1991) "Efficient pseudopotentials for plane-wave calculations", *Phys. Rev. B* **43**, 1993.
[15] Kobayashi, K. (2001) "A Database for Norm—Conserving Pseudopotential (NCPS2K): Application to rare gas atoms", Materials Transactions, **42**(No. 11), 2153. Please see "http://www.nims.go.jp/ cmsc/fps2/INFO/sanzene.html".
[16] Kleinman, L. and Bylander, D.M. (1982) "Efficacious form for model pseudopotentials", *Phys. Rev. Lett.* **48**, 1425.
[17] Louie, S.G., Froyen, S. and Cohen, M.L. (1982) "Nonlinear ionic pseudopotentials in spin-density-functional calculations", *Phys. Rev.* **B26**, 1738.
[18] Car, R. and Parrinello, M. (1985) "Unified approach for molecular dynamics and density-functional theory", *Phys. Rev. Lett.* **55**, 2471.
[19] Williams, A.R. and Soler, J. (1987), *Bull. Am. Phys. Soc.* **32**, 562.
[20] Nielsen, O.H. and Martin, R.M. (1985) "Stresses in semiconductors: Ab initio calculations on Si, Ge, and GaA", *Phys. Rev. B* **32**, 3792.
[21] Wörle, M., Nesper, R., Mair, G., Schwarz, M. and Schnering, H.G. von (1995) "LiBC—a completely intercalated heterographite", *Z. Anorg. Allg. Chem.* **621**, 1153.
[22] Kobayashi, K. and Yamamoto, K. (2002) "Electronic and lattice properties of MgB_2 under *a*, *b*-axis compression", *J. Phys. Soc. Jpn.* **71**, 397.